Ocean Engineering 104 (2015) 129–139

Contents lists available at ScienceDirect

Ocean Engineering

journal homepage: www.elsevier.com/locate/oceaneng

Network dynamic stability of floating airport based on amplitude death

H.C. Zhang [a], D.L. Xu [a,*], C. Lu [a], S.Y. Xia [a], E.R. Qi [b], J.J. Hu [b], Y.S. Wu [b]

[a] State Key Laboratory of Advanced Design and Manufacturing for Vehicle Body, College of Mechanical and Vehicle Engineering, Hunan University, Changsha 410082, PR China
[b] China Ship Scientific Research Center, Wuxi 214082, PR China

ARTICLE INFO

Article history:
Received 10 February 2015
Accepted 9 May 2015

Keywords:
Floating airport
Network dynamics
Amplitude death
Nonlinear

ABSTRACT

A large scale floating airport, consisting of multi-modules coupled with flexible connectors, can be viewed as a dynamic network. The special dynamic behavior of amplitude death, a suppressed weak oscillatory state, is studied by using the nonlinear network theory. A generalized network model is established for the floating airport, and an analytical solution of its response is formulated. A semi-analytical method is employed to analyze the amplitude death phenomenon and then a critical condition is derived. The parameter domain for the onset of the amplitude death is obtained by numerical simulations which match well with the analytical results. The work provides a typical application of the network theory in the marina engineering and illustrates the importance of amplitude death mechanism in the stability design of very large floating structures.

1. Introduction

With growing population and expansion of urban development, engineers have proposed the construction of very large floating structures (VLFS) for industrial space, floating airport, storage facilities and even habitation because of the distinct advantages of relatively simple construction and ease of maintenance (Watanabe et al., 2004; Cui et al., 2007). Design and construction for VLFS have been discussed and studied to some extent at least as far back as 1924 that Edward R. Armstrong patented the Sea Station to be used as airplane supply and navigating stations (Armstrong, 1924). The Sea Station was to serve as refueling airfields at sea in Armstrong Seadrome for transatlantic aircraft hauling freight and passengers between the United States and Europe (Armstrong, 1943). However, the enthusiasm for building these floating structures was dampened due to very high cost and failure to address security concerns. It was not until 1970s that the VLFS technology was revived and developed further by the Japanese to create a floating airport for the Kansai International Airport (Wang and Tay, 2011). Although the Kansai airport did not adopt the floating airport design, the research and development exercise prepared the Japanese engineers and naval architects to build the Mega-Float in Tokyo Bay in 1995 as a test floating runway. Different from the pontoon-type proposed by Japanese, the US navy also proposed mobile offshore base (MOB) which consists of several semi-submersible modules with a total length of about 5000 ft in the late1999s to support military operations where conventional land bases were not available (Bhattacharya et al., 2006). Apart from Japan and USA, other countries such as Norway (Faltinsen, 1996; Rognaas et al., 2001), the United Kingdom (Taylor and Waite, 1978), Netherlands (Pinkster and Fauzi, 1997), China (Chen et al., 2001; Fu et al., 2007), Korea (Hong et al., 1999) and Singapore (Koh and Lim, 2009) have carried out researches on VLFS. Design of large scale floating airport is difficult, because it has to satisfy stringent functional and operational requirements (Gao et al., 2011). For example, the maximum pitch angle between modules must be less than about 0.86° for the aircraft operation on Mobile Offshore Base in Sea State 6 (Rognaas et al., 2001). So the stringent tolerance on the deformation of the floating structure requires relatively precise prediction on dynamic responses in the design stage.

Due to massive size of the VLFS, methods of dynamic prediction are very much different from that of other marine structures. Based on flat structure characteristic of floating airport, some scholars adopted the beam or plane models, including the hydroelastic effect to analyze the dynamic responses (Aoki, 1997; Hamamoto, 1994; Kashiwagi, 1998; Khabakhpasheva and Korobkin, 2001; Kim and Ertekin, 1998). These simplified models are only suitable for the pontoon type VLFS. In general, since the

* Correspondence to: College of Mechanical and Vehicle Engineering, Hunan University, Yuelu District, Changsha City, Hunan Province, P.R. China. Tel.: +86 731 88821791; fax: +86 731 88822051.
E-mail address: dlxu@hnu.edu.cn (D.L. Xu).

http://dx.doi.org/10.1016/j.oceaneng.2015.05.008
0029-8018/

VLFS has much larger horizontal dimensions than the vertical one, it is usually constructed by connecting multiple standardized modules with connectors for easy construction, transportation and deployment (Watanabe et al., 2004). For the multi-modules floating structures, the simplified beam or plate models are no longer suitable due to the effect of the stiffness of flexible connector. Considering the stiffness of the flexible connector between the adjacent modules which is much less than the stiffness of the module structure itself, some scholars proposed hinged elastic beam or plate models (Du and Ertekin, 1991; Lee and Newman, 2000; Maeda et al., 1979; Riggs and Ertekin, 1993) and dynamics predictions were carried out by using linearized modal superposition or finite element discretization methods. We stress that linearlization methodology could generally fail to analyze the true dynamics of VLFS. Due to the considerable differences in the scale sizes between the floating modules and flexible connectors, small displacements of the floating modules may cause very large displacements at joints of connectors, which gives rise to strongly geometrical nonlinearity when establishing the connector model. Xu et al. (2014a) and Zhang et al. (2015) reported that the nonlinear stiffness of connectors may significantly amplify the module responses through jumping phenomena, which the linear methods cannot reveal.

The floating airport under consideration in this paper consists of multiple modules that are coupled with flexible connectors in a chain topological form. Each floating module can be viewed as an oscillator in waves and the connector between adjacent modules can be viewed as a coupling. Thus the integrated platform becomes a typical dynamic network system in which the nonlinearity may be derived from fluid–structure interaction, elastic material properties or geometric nonlinearity of the flexible connectors. The dynamic characteristics may involve complex network dynamic phenomena such as synchronization, hysteresis, phase lock and shift (Kaneko, 1993; Ott, 2002; Pecora and Carroll, 1990). Among the remarkable phenomena, amplitude death refers to the dynamic stability for the network structure system (Bar-Eli, 1984). Different from the traditional concept of stability, amplitude death means that the oscillation of all oscillators in the network system collectively tends to zero motion in autonomous networks (Saxena et al., 2012) or a suppressed weak oscillatory state in non-autonomous networks (Resmi et al., 2011) due to the interaction among coupled oscillators. Amplitude death is a typical stationary state for nonlinear network systems.

In this paper, we investigate a special dynamic behavior of the suppressed weak oscillatory state of a floating airport based on the mechanism of amplitude death because it is important for the stability design of the floating airport and load reduction in flexible connectors. Our recent works (Xu et al., 2014a; Zhang et al., 2015) pioneered the application of network theory to the nonlinear dynamics prediction of the floating airport, and preliminarily investigate the complex nonlinear dynamic phenomena of the floating airport in two degrees of freedom of the surge and heave motions. The results indicated that the traditional methods may greatly underestimate the actual responses and loads on the structure of the floating airport (Xu et al., 2014c). The previous works (Xu et al., 2014a; Zhang et al., 2015) mainly explored the feasibility of the new methodology and did not cover a complete and strict mathematic explanation for the important phenomenon of amplitude death. This paper gives a full explanation of amplitude death and further extends the floating airport model to the three degrees of freedom including surge, heave and pitch motions. A new model of rubber-cable connector is adopted. A chain-type nonlinear network dynamic model of floating airport is formulated based on the linear wave theory, a dynamic model of single floating module, a coupling model of the new connector and a constraint model of a mooring system. A semi-analytical critical condition of amplitude death is derived by using an averaging method. Based on the mechanism of amplitude death, we investigate the parametric domain for the suppressed weak oscillatory state of the floating airport and the results can be used as a theoretical guideline for the stability design of the floating airport. It is worthy to notice that the methodology of network dynamic theory applied in this paper can be extensible to many engineering problems with similar network structures.

2. Network model of floating airport

The sketch of the chain-type floating airport is shown in Fig. 1 in which the original point of global coordinates is set in free surface, the x-axis is on the undisturbed free-surface and the z-axis is upwards. The network model of the multi-module floating airport is to be integrated by using the dynamic model of a single floating body and coupling model of connector and the constraint model of the mooring system.

2.1. Model of a single floating body

In this paper, the floating modules are considered as rigid bodies and the surge, heave and pitch motions are considered. The mathematic model of the i-th module can be formulated by *Cummins Equation* (Taghipour et al., 2008) using a linear wave theory (Stoker, 2011),

$$(\mathbf{M}_i+\boldsymbol{\mu}_i)\ddot{\mathbf{X}}_i+\boldsymbol{\lambda}_i\dot{\mathbf{X}}_i+\mathbf{S}_i\mathbf{X}_i=\mathbf{F}_{iW}+\mathbf{F}_{iC}+\mathbf{F}_{iM} \tag{1}$$

where $\mathbf{X}_i=[x_i,z_i,\beta_i]^T$ denotes the generalized displacement for surge, heave and pitch motions of i-th module. $\mathbf{M}_i$, $\mathbf{S}_i$ indicate the mass and hydroelastic restoring matrix, written as

$$\mathbf{M}_i=\begin{bmatrix} m & 0 & m(z_c-z_g) \\ 0 & m & -m(x_c-x_g) \\ m(z_c-z_g) & -m(x_c-x_g) & I_{xx}^V+I_{zz}^V \end{bmatrix} \tag{2}$$

$$\mathbf{S}_i=\begin{bmatrix} 0 & 0 & 0 \\ 0 & \rho g A_W & -\rho g I_x^W \\ 0 & -\rho g I_x^W & \rho g(I_{xx}^W+I_{zz}^W)-mg(z_c-z_g) \end{bmatrix} \tag{3}$$

where m is the mass of the single module, A_W denotes the area of

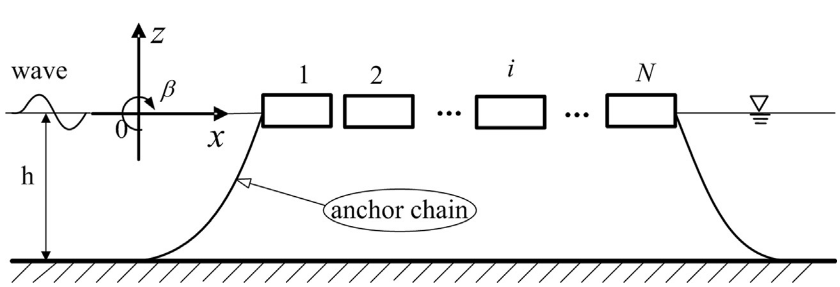

Fig. 1. Sketch for the multi-module floating airport.

water plan satisfied $A_W = L$ for the two dimensional problem. $(x_c, z_c)$and (x_g, z_g) indicate the coordinates of the rotation and mass center respectively. V is the volume of submerged module which satisfied $V = Ld$, where L and d denote the length and sub-depth of module. The first and second moments of inertia of water plane area and submerged volume with respect to the rotation center $I_x^W, I_{xx}^W, I_{zz}^W, I_{xx}^V, I_{zz}^V$ are defined as below (Sannasiraj et al., 2001)

$$I_{xx}^V = \iint_V (x-x_c)^2 dm,\ I_{zz}^V = \iint_V (z-z_c)^2 dm,\ I_x^W = \int_{A_W} (x-x_c) dA,\ I_{xx}^W = \int_{A_W} (x-x_c)^2 dA,\ I_{zz}^W = \iint_{A_W} (z-z_c)^2 dm.$$

The classical linear wave theory is commonly used to formulate the hydrodynamic model in which the wave potential can be divided into incident potential, scattered potential and radiation potential (Stoker, 2011). The matrices $\boldsymbol{\mu}$, $\boldsymbol{\lambda}$ in Eq. (1) represent the added mass and the added damping respectively as a result of the radiation potential due to the motion of the module, and their elements can be determined by using the eigenfunction expansion matching method when wave frequency is given (Zheng et al., 2004). The incident and diffraction wave potential mainly contribute to the periodic excitation force, while the effect of scattered wave potential is not considered here for the reason of simplicity. As the main purpose of this work is to elaborate the special dynamic phenomenon of amplitude death of the floating airport, we attempt to keep all models simple, including the wave model. For a head wave of height a and wave regular frequency ω, the wave force $\mathbf{F}_{iW}$ imposed on the i-th floating module is written as

$$\mathbf{F}_{iW} = \left[f_{wx}, f_{wz}, f_{w\beta}\right]^T \exp(-i\omega t) \tag{4}$$

where $i = \sqrt{-1}$ and the force amplitude$f_{wx}, f_{wz}, f_{w\beta}$ can be obtained by integrating the incident potential along its wet surface, formulated as

$$\begin{aligned} f_{wx} &= 2\rho g a \sin(kL/2) \frac{\mathrm{sh}kh - \mathrm{sh}k(h-d)}{k\mathrm{ch}kh} \\ f_{wz} &= 2\rho g a \sin(\frac{kL}{2}) \frac{\mathrm{ch}k(h-d)}{k\mathrm{ch}kh} \exp(i\pi/2) \\ f_{w\beta} &= -\omega\rho a \times \left(\begin{array}{l} \frac{2\sin(kL/2)}{k^2\mathrm{ch}kh}(kd\mathrm{sh}k(h-d) + \mathrm{ch}k(h-d) - \mathrm{ch}kh) \\ + \frac{\mathrm{ch}k(h-d)}{k^2\mathrm{ch}kh}(kL\cos(kL/2) - 2\sin(kL/2)) \end{array} \right) \end{aligned} \tag{5}$$

Since the hydrodynamic model of the single module is a well-developed method, only the relevant references are cited for further reading without involving detailed mathematic derivations.

The last two terms of $\mathbf{F}_{i,C}, \mathbf{F}_{i,M}$ in the right handside of Eq. (1) indicate the connector force and the force produced by mooring system to be derived later.

2.2. Coupling model of connectors

Connectors are the key elements that play an important role in dynamic responses of the floating airport. This coupling model in fact describes the force–deformation relationship of the connector associated with module positions. Traditional methods simply assign linear stiffness for connectors in each direction of the motion, and truncate the important effect of nonlinearity. It is worthy to notice that the nonlinearity could be caused not only by the material property but also by the geometric configuration of the connector. The geometric nonlinearity is induced by the large displacements at connection points, because small pitch motions of the modules could lead to significant displacements at the connection joints due to the huge scale of the modules.

In this paper, a rubber–cable connector is considered where the cable holds linear property and the rubber possesses cube property in stiffness, shown in Fig. 2(a).

In Fig. 2(a), the blue block marked with width δ is two trapezoid rubbers, two elastic cables are tied with adjacent modules in parallel with distance δ_2 and the initial length of the cable is δ. In this connector model, we assume that the rubber only constrains the compressive motion (the shearing deformation ignored) and the cable constrains departure motions of floating modules.

The floating modules are considered as rigid bodies and the surge, heave and pitch motions are considered. The origin of the local coordinate for each floating module is set at the rotation center of floating module, $X_i$axis is parallel with undisturbed free-surface and Z_i axis points upwards. The relationship between initial and deformation positions of the adjacent modules is shown in Fig. 2(b).

We simplify the adjacent modules as two triangles. The solid circles denote the rotation centers of the adjacent modules and the hollow circles denote the hinge joints between which the solid lines labeled with C_{ij}^1, C_{ij}^2 denote the connectors. The dashed line triangle denotes the initial position and the solid line represents the position after deformation with the displacement (x_i, z_i, β_i) and (x_j, z_j, β_j). The pitch angle β of each module is a small quantity due to the huge scale of the module, so that

$$\sin\beta \doteq \beta, \qquad \cos\beta \doteq 1 \tag{6}$$

In what follows, we will formulate the mechanical model of the coupled connectors based on the approximation of Eq. (6). Considering the geometric relationship of adjacent modules, the deformation of cables $\Delta l_{ij}^{(k)}$ $(k = 1, 2)$ are formulated as

$$\Delta l_{ij}^{(k)} = \begin{cases} 0, & l_{ij}^{(k)} - \delta \le 0 \\ l_{ij}^{(k)} - \delta, & l_{ij}^{(k)} - \delta > 0 \end{cases} k = 1, 2 \tag{7}$$

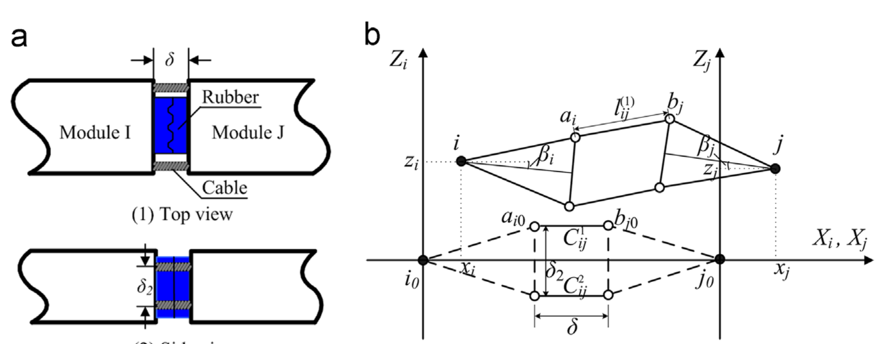

Fig. 2. (a) Sketch for the connecter. (b) The position relationship for adjacent modules. (For interpretation of the references to color in this figure, the reader is referred to the web version of this article.)

where

$$l_{ij}^{(1)}=\sqrt{\left[\mathrm{sgn}(j-i)\delta+\frac{\delta_2}{2}(\beta_j-\beta_i)+x_j-x_i\right]^2+\left[\mathrm{sgn}(j-i)\frac{L}{2}(\beta_j+\beta_i)+z_j-z_i\right]^2},$$

$$l_{ij}^{(2)}=\sqrt{\left[\mathrm{sgn}(j-i)\delta-\frac{\delta_2}{2}(\beta_j-\beta_i)+x_j-x_i\right]^2+\left[\mathrm{sgn}(j-i)\frac{L}{2}(\beta_j+\beta_i)+z_j-z_i\right]^2}.$$

The direction vector for the projection of the cables deformation is formulated as

$$\mathbf{n}_{ij}^{(k)}=\Theta_{ij}^{(k)}\mathbf{i}+\Pi_{ij}^{(k)}\mathbf{j} \tag{8}$$

where $\mathbf{i},\mathbf{j}$ denote the unit vector of x,z axis and $\Theta_{ij}^{(k)},\Pi_{ij}^{(k)}$ denote the deformation coefficients in the surge and heave directions, respectively,

$$\Theta_{ij}^{(1)}=\frac{\mathrm{sgn}(j-i)\delta+\delta_2(\beta_j-\beta_i)/2+x_j-x_i}{l_{ij}^{(1)}}$$

$$\Pi_{ij}^{(1)}=\frac{\mathrm{sgn}(j-i)L_i(\beta_j+\beta_i)/2+z_j-z_i}{l_{ij}^{(1)}}$$

$$\Theta_{ij}^{(2)}=\frac{\mathrm{sgn}(j-i)\delta-\delta_2(\beta_j-\beta_i)/2+x_j-x_i}{l_{ij}^{(2)}}$$

$$\Pi_{ij}^{(2)}=\frac{\mathrm{sgn}(j-i)L_i(\beta_j+\beta_i)/2+z_j-z_i}{l_{ij}^{(2)}} \tag{9}$$

The arms of force imposed on the rotation center of i-th module due to cable forces are formulated as

$$\mathbf{r}_{ij}^{(k)}=r_{ijx}^{(k)}\mathbf{i}+r_{ijz}^{(k)}\mathbf{j} \tag{10}$$

where

$$r_{ijx}^{(1)}=\mathrm{sgn}(j-i)L_i/2+\delta_2\beta_i/2,\ r_{ijz}^{(1)}=\delta_2/2-\mathrm{sgn}(j-i)L_i\beta_i/2$$
$$r_{ijx}^{(2)}=\mathrm{sgn}(j-i)L_i/2-\delta_2\beta_i/2,\ r_{ijz}^{(2)}=-\delta_2/2-\mathrm{sgn}(j-i)L_i\beta_i/2 \tag{11}$$

The vector diameters of moment imposed on the rotation center of i-th module due to the cable forces are formulated as

$$\mathbf{m}_{ij}^{(k)}=\mathbf{r}_{ij}^{(k)}\times\mathbf{n}_{ij}^{(k)}=\Upsilon_{ij}^{(k)}\mathbf{k} \tag{12}$$

where $\mathbf{k}$ denotes the unit vector of y axis and $\Upsilon_{ij}^{(k)}$ denotes the deformation coefficients in the pitch direction, substituting Eqs. (8) and (10) into Eq. (12), we obtained

$$\Upsilon_{ij}^{(k)}=\Theta_{ij}^{(k)}r_{ijz}^{(k)}-\Pi_{ij}^{(k)}r_{ijx}^{(k)} \tag{13}$$

In this paper, we assume that a single cable connector has a linear stiffness k_c along its longitudinal direction, thus the cable force of the combined connectors imposed on the i-th module gives,

$$\mathbf{F}_{ij}^{c}=k_c\begin{bmatrix}\Delta l_{ijx} & \Delta l_{ijz} & \Delta l_{ij\beta}\end{bmatrix}^T \tag{14}$$

where

$$\Delta l_{ijx}=\Delta l_{ij}^{(1)}\Theta_{ij}^{(1)}+\Delta l_{ij}^{(2)}\Theta_{ij}^{(2)},\quad \Delta l_{ijz}=\Delta l_{ij}^{(1)}\Pi_{ij}^{(1)}+\Delta l_{ij}^{(2)}\Pi_{ij}^{(2)},$$
$$\Delta l_{ij\beta}=\Delta l_{ij}^{(1)}\Upsilon_{ij}^{(1)}+\Delta l_{ij}^{(2)}\Upsilon_{ij}^{(2)} \tag{15}$$

The deformation of the rubber Δr_{ij} is formulated as

$$\Delta r_{ij}=\begin{cases}x_j-x_i, & \mathrm{sgn}(j-i)(x_j-x_i)<0\\ 0, & \mathrm{sgn}(j-i)(x_j-x_i)\ge 0\end{cases} \tag{16}$$

In this paper, we assume that the rubber has a cubic stiffness k_r, the rubber force imposed on the i-th module gives,

$$\mathbf{F}_{ij}^{r}=k_r\begin{bmatrix}\Delta r_{ij}{}^3 & 0 & 0\end{bmatrix}^T \tag{17}$$

By now, the mechanical model for the coupled rubber–cable connector is formulated in Eqs. (14) and (17). Note that the model of the combined connector has a piecewise nonlinear characteristic which contains geometric nonlinearity in Eq. (14) and the material nonlinearity in Eq. (17). It is worth to notice that the hinge points have very large displacements even if the pitch angles of the modules are small due to the massive scale of the modules. Thus the connector model of cable has strong nonlinearity.

2.3. Constraint model of mooring system

The floating structure is practically constrained by a mooring system to prevent drifting. In this paper, we chose the slack mooring line as the mooring system in our model. The mooring line tension acting on the floating module is represented as a linear function of displacement by using integrated equations of deep sea mooring lines in a static equilibrium (Ogawa, 1984). The derivation for the linearized stiffness coefficients of the mooring matrix $\mathbf{K}$ follows the simplified method suggested by Jain (Jain, 1980). It assumed that the mooring line is perfect flexible, inextensible and heavy.

The sketch showing a two dimensional floating structure moored by catenary line of length H is shown in Fig. 3. The mooring line is anchored at point B with a bottom angle θ_0 and the other end is attached at point Q of the floating module. The catenary line is extended hypothetically beyond B for a length l to B', so that the angle θ at B' is zero. Two sets of rectangular coordinates(ξ,ϑ) and (χ,Ω) are chosen in the plane of the catenary line through B and B', respectively.

In the coordinate system (χ,Ω),the initial horizontal and vertical tensions of the catenary line can be written as

$$U_h=U\cos\theta=U_0$$
$$U_v=U\sin\theta=ws \tag{18}$$

where U denotes the catenary line tension, w is unit weight of catenary line, U_0 denotes initial horizontal catenary tension. s is the total arc length of catenary line measured from point B'.

The basic catenary line equations are formulated as

$$\chi=(U_0/w)\sinh^{-1}(ws/U_0)$$
$$\Omega=(U_0/w)\left\{\left[1+(ws/U_0)^2\right]^{1/2}-1\right\} \tag{19}$$

Thus coordinates of points Q,B in the (χ,Ω) coordinate system can be written as

$$\chi_Q=(U_0/w)\sinh^{-1}(w\overline{H}/T_0)$$
$$\Omega_Q=(U_0/w)\left\{\left[1+(w\overline{H}/U_0)^2\right]^{1/2}-1\right\} \tag{20}$$

$$\chi_B=(U_0/w)\sinh^{-1}(wl/U_0)$$
$$\Omega_B=(U_0/w)\left\{\left[1+(wl/U_0)^2\right]^{1/2}-1\right\} \tag{21}$$

where $\overline{H}=H+l$, and the catenary line tension at point Q,B can be formulated as

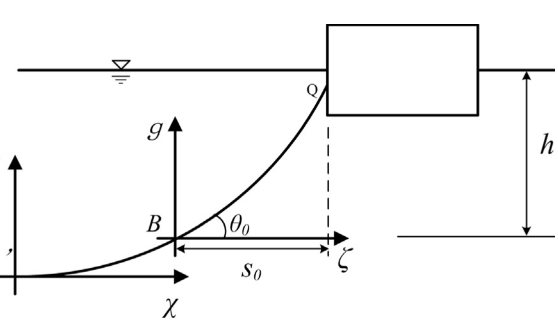

Fig. 3. Coordinate diagram of mooring line.

$$U_Q = U_0\left[1+(w\overline{H}/U_0)^2\right]^{1/2} \tag{22}$$

$$U_B = U_0\left[1+(wl/U_0)^2\right]^{1/2} \tag{23}$$

Thus, the linearized stiffness coefficients can be formulated as (Sannasiraj et al., 1998)

$$K_{12} = U_0\left\{w\left(\frac{U_B\overline{H}-U_Q l}{U_Q-U_B}\right)\left[\frac{\zeta_Q}{U_0}-\left(\frac{U_B\overline{H}-U_Q l}{U_Q U_B}\right)\right]-\frac{U_0{}^2\vartheta_Q}{U_Q U_B}\right\}^{-1} \tag{24}$$

$$K_{11} = \frac{w}{U_0}\left(\frac{U_B\overline{H}-U_Q l}{U_Q-U_B}\right)K_{12} \tag{25}$$

$$K_{22} = \frac{w}{U_0}\left(\frac{U_B U_Q}{U_Q-U_B}\right)\left[\frac{\zeta_Q}{U_0}-\left(\frac{U_B\overline{H}-U_Q l}{U_Q U_B}\right)\right]K_{12} \tag{26}$$

$$K_{13} = \left[\frac{wZ_Q}{U_0}\left(\frac{U_B\overline{H}-U_Q l}{U_Q-U_B}\right)-X_Q\right]K_{12} \tag{27}$$

$$K_{23} = \left\{Z_Q-\frac{wX_Q}{U_0}\left(\frac{U_B U_Q}{U_Q-U_B}\right)\left[\frac{\zeta_Q}{U_0}-\frac{U_B\overline{H}-U_Q l}{U_Q U_B}\right]\right\}K_{12} \tag{28}$$

$$K_{33} = \left\{\frac{wZ_Q{}^2}{U_0}\left(\frac{U_B\overline{H}-U_Q l}{U_Q-U_B}\right)-\frac{wX_Q{}^2}{U_0}\left(\frac{U_B U_Q}{U_Q-U_B}\right)\left[\frac{\zeta_Q}{U_0}-\frac{U_B\overline{H}-U_Q l}{U_Q U_B}\right]\right.$$
$$\left.-2X_Q Z_Q\right\}K_{12} \tag{29}$$

where (X_Q, Z_Q) is the coordination of the attachment point Q in the local coordinate shown in Fig. 2. Also the mooring matrix is symmetric, namely$K_{ij}=K_{ji}, i=1,2,3; j=1,2,3$.

Generally, the length H of mooring line, project length s_0 and water depth $h$are known. The initial horizontal tension T_0, anchor angle θ_0 and hypothetical projected length l can be evaluated from the Eq. (18) for catenary line tension and the basic catenary line Eq. (19). And then, the mooring stiffness matrix can be calculated using Eqs. (24)–(29). Thus the force of mooring lines imposed on floating modules can be defined as

$$\mathbf{F}^m = -\mathbf{KX} \tag{30}$$

2.4. Network dynamics model of floating airport

In this section, we will integrate all the models derived above to form the network dynamic model of N modules floating airport. For computing the total connector loads imposed on the i-th module, we introduce a topology matrix Φ to deal with arbitrary connection among the floating modules. The element Φ_{ij} of topology matrix Φ is set to 1 when the i-th module connects with the j-th module, otherwise Φ_{ij} is set to zero. The diagonal element Φ_{ii} is set to zero, meaning that a module cannot connect with itself. Referring to the model of the rubber–cable connector described in Eqs. (14) and (17), the total force imposed on i-th module can be formulated as

$$\mathbf{F}_{iC} = \varepsilon_1\sum_{j=1}^{N}\Phi_{ij}G_1(\mathbf{X}_i,\mathbf{X}_j)+\varepsilon_2\sum_{j=1}^{N}\Phi_{ij}G_2(\mathbf{X}_i,\mathbf{X}_j) \tag{31}$$

The two terms in the right hand side of Eq. (31) represent the physical features of the coupling among adjacent modules. The parameters $\varepsilon_1, \varepsilon_2$ denote coupling strengths which correspond to the stiffness of the rubber and the cable, respectively. $G_1(\mathbf{X}_i,\mathbf{X}_j)$ and $G_2(\mathbf{X}_i,\mathbf{X}_j)$ are the coupling functions which describe the coupling characteristics of the connector, given as

$$G_1(\mathbf{X}_i,\mathbf{X}_j) = \left[\Delta r_{ij}{}^3, 0, 0\right]^T \tag{32}$$

$$G_2(\mathbf{X}_i,\mathbf{X}_j) = \left[\begin{matrix}\Delta l_{ijx} & \Delta l_{ijz} & \Delta l_{ij\beta}\end{matrix}\right]^T \tag{33}$$

where the expressions of symbols $\Delta r_{ij}, \Delta l_{ijx}, \Delta l_{ijz}, \Delta l_{ij\beta}$ have been given in Eqs. (15) and (16). Note that the coupling function in Eq. (32) describes the material nonlinearity, and the coupling function in Eq. (33) describes the geometric nonlinearity, different from the linear stiffness assumption (Riggs et al., 1999). From the perspective of network dynamics, the piecewise nonlinear coupling in Eqs. (32) and (33) is different from the delay coupling (Strogatz, 1998) and the dynamic coupling (Konishi, 2003).

Introduction of the topology matrix into the dynamics model enables to deal with the arbitrary connection of modules, which results in diverse types of topological network structures by only changing the element assignment. For the different types of topology network, such as a ring form or a rectangular form, we can formulate the models only by assigning the elements value of the topology matrix accordingly. For the chain-type network model of the floating airport, the topology matrix Φ_{ij} is symmetric, given by

$$\Phi_{ij} = \begin{cases}1 & j=i+1\\ 0 & others\end{cases} \quad i=1,2,\cdots,N;\quad j=i,i+1,\cdots,N \tag{34}$$

Considering the simplest linear mooring model derived above in Eq. (30), the mooring force imposed on the i-th module can be written as

$$\mathbf{F}_{iM} = -\mathbf{K}_i\mathbf{X}_i \tag{35}$$

For a chain-type floating airport consisting of N floating modules coupled by flexible connectors, based on a single floating model in Eq. (1) with consideration of coupling effects of connector model in Eq. (31) and the constraint model of mooring system in Eq. (35), the network dynamic model can be formulated as

$$(\mathbf{M}_i+\boldsymbol{\mu}_i)\ddot{\mathbf{X}}_i+\boldsymbol{\lambda}_i\dot{\mathbf{X}}_i+(\mathbf{K}_i+\mathbf{S}_i)\mathbf{X}_i = \mathbf{F}_{iW}\exp(-i\varphi_i)$$
$$+\varepsilon_1\sum_{j=1}^{N}\Phi_{ij}G_1(\mathbf{X}_i,\mathbf{X}_j)+\varepsilon_2\sum_{j=1}^{N}\Phi_{ij}G_2(\mathbf{X}_i,\mathbf{X}_j),\quad i=1,\cdots,N \tag{36}$$

The first term on the right hand side of Eq. (36) denotes wave forces imposed on the i-th module. When a head wave propagates along the huge size of the floating airport, the wave forces imposed on the adjacent modules have a phase delay $\Delta\varphi_{i(i+1)} = \varphi_{i+1}-\varphi_i = k(L_i+L_{i+1})/2$, where φ stands for phase angle, subscript i represents the i-th module.

By now, the network dynamic model of chain-type floating airport with flexible connectors is developed. The nonlinearity is resulted from of the connector model. The network model Eq. (36) stands for a generalized model which is feasible to describe the dynamics of multi-module floating structures in arbitrary topology shapes.

3. Amplitude death of floating airport

Different from the traditional concept of stability, we investigate the special stability state for the floating airport based on amplitude death mechanism. The phenomenon of amplitude death is illustrated by numerical simulation to understand its physical meaning of dynamic stability for the floating airport. Then the mechanism of the amplitude death is investigated using an averaging method and furthermore the critical condition is derived. In the end, the parametric domain for the emergence stationarity of the floating airport is given based on amplitude death mechanism.

3.1. Phenomenon of amplitude death

A floating airport is constructed by serially connecting multiple floating modules in waves. For the convenience to illustrate the behaviors of the floating airport, an airport model consisting of 5 modules is considered. The box-type is chosen for a single floating module and its property is listed in Table 1.

Table 1
Property of single floating module.

Length L(m)	Height D(m)	Sub-depth d(m)	Linear density m_0(kg /m)
200	8	5	5125

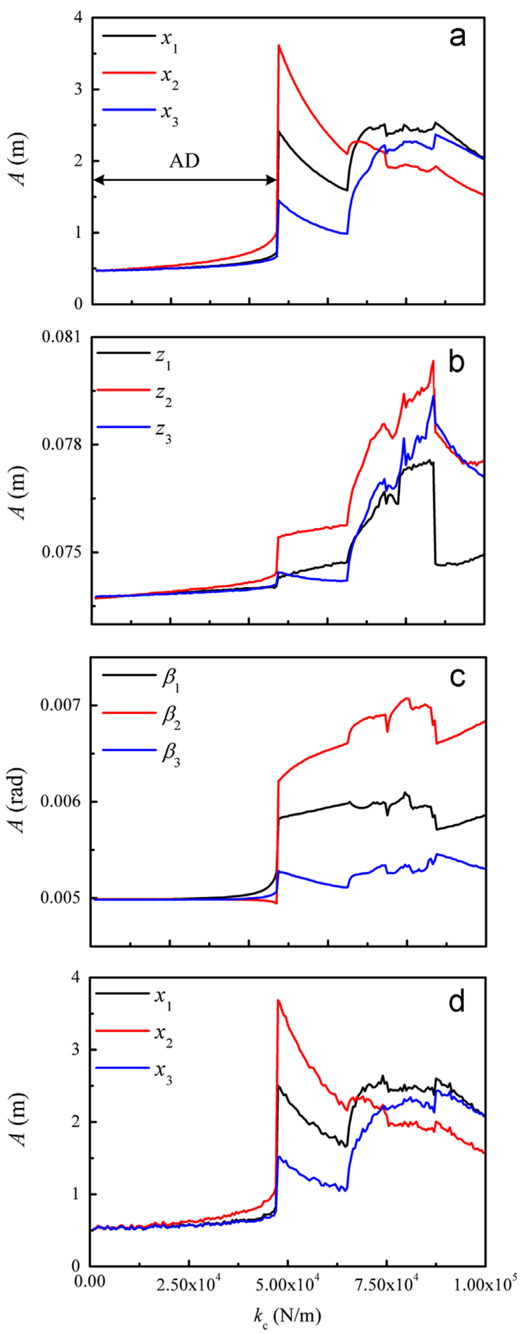

Fig. 4. The response amplitude versus coupling strength of (a) surge motion, (b) heave motion,(c) pith motion and (d) surge motion after adding GWN noise in the wave period $T=10$ s.

The distance between adjacent modules and the initial length of the connector are set as $\delta=5$ m, the vertical distance between parallel cables is $\delta_2=5$ m. Considering that the difference between the two stiffnesses of the rubber and cable should not be large, we introduce a coupling strength ratio $\eta(0<\eta<1)$ that is the stiffness ratio of the rubber over the cable. For this simulation, the coupling strength ratio is $\eta=0.6$. The parameters of sea conditions are set with wave height $a=3$ m, namely the 5th sea state, and water depth $h=50\ m$, wave period $T=10$ s. The parameters for the mooring system are set at the unit weight of catenary line $w=3253.6\ N/m$, length $H=350\ m$, project length $s_0=310\ m$ (Winkler et al., 1990) and coordinates of the attachment point $(X_Q, Z_Q)=(\pm 100, 0)$.

Fig. 4 illustrates the responses of surge, heave and pith versus cable stiffness k_c. From Fig. 4(a)–(c), we see that the responses in all degrees of freedom for all modules are relatively weak when the coupling strength $k_c<4.71\times10^4\ N/m$ and the amplitudes are simultaneously amplified at a critical value of coupling strength $k_c=4.71\times10^4\ N/m$. Compared with the different modules, the amplitudes of different module are almost the same before jumping up but after that diverse differently for the parameter region of large oscillation especially for the surge freedom. According to the definition for amplitude death as noted by Resmi et al. (2011) for non-autonomous system, the low-level oscillation state for the interval of $0<k_c<4.71\times10^4\ N/m$ is regarded as an amplitude death which corresponds to the calm state for the floating airport. In comparison with the state of the amplitude death and the large oscillation amplitude for the surge motion is amplified more than 4 times after the jumping phenomenon occurs, which extremely threatens the safety of the floating airport. For real sea condition, the wave form could be complex involving wave noise or even completely stochastic process (Kerman, 1988). However, the stochastic process analysis for high-dimensional nonlinear systems does not have a full-fledged method. Thus our work does not include stochastic analysis. In order to illustrate the weak wave noise effect on our results, a simple example for added wave noise is illustrated in Fig. 4(d). A zero-mean weak Gauss White Noise (GWN) $G(t)$ with signal to noise ratio (SNR) $\eta=70$ db is added to Eq. (36). The resulting evolution of the surge motion does not change much in the studied range of stiffness k_c and the jump point is almost the same compared with Fig. 4(a) without noise. In the noise case the amplitude curve becomes non-smooth in the varying region of k_c even if in the amplitude death region. Above analysis clarifies that the weak wave noise cannot affect the characteristic response significantly.

The similar results can be observed from the connector loads. Fig. 5 shows the connector loads versus coupling strength where the cable load and the rubber load marked with C, R rise up significantly after the end of amplitude death state.

From Fig. 5, the connector loads have the similar evolution pattern with the response of surge motion. The loads of connectors in symmetrical location are equivalent. The rubber load is larger than the cable load at the same parameters. Similarly, the connector loads are all relatively small in the internal of $k_c<4.71\times10^4\ N/m$ where the amplitude death state exists. The rubber and cable loads are amplified at the critical of $k_c=4.71\times10^4\ N/m$ at which the response experiences a jumping up event. The connector load is amplified almost 5 times at the critical parameter. We remark that the state of amplitude death (weak oscillation state) is a great concern because it makes the system remain in a calm state meanwhile keeps the connector load at low level. By observing the weak oscillation state, we found that the weak oscillation follows the wave frequency.

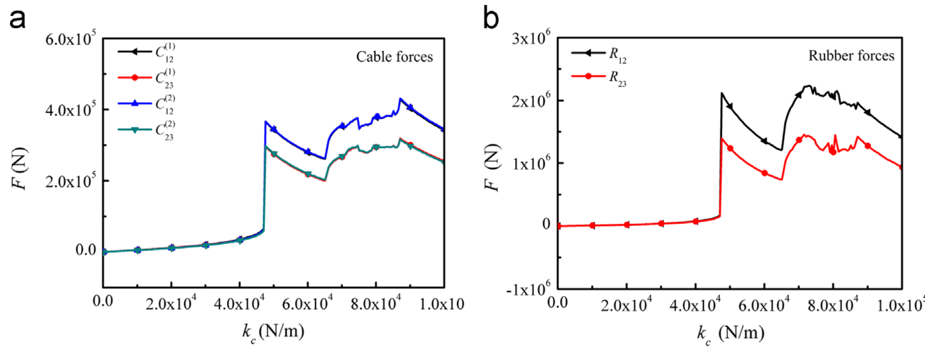

Fig. 5. Connector load evolution under the coupling strength of (a) cable loads and (b) rubber loads with wave period $T=10$ s.

After having simulated many other cases not reported here, we can conclude the following features in common. (1) The weak oscillation state namely amplitude death widely exists for the multi-module floating airport with flexible connector. (2) Based on the synergetic effect of network, the amplitude jumping phenomenon happens simultaneously among all modules, which means that different modules share the same parameters domain of amplitude death. (3) The frequency of the weak oscillation state is always identical to the wave frequency. The determination of parameters domain for amplitude death is significant for the global dynamic stability of the multi-module floating airport and its safety design of flexible connectors.

3.2. Analytical solution for weak oscillation state

With the clue of the equivalence between the weak oscillation period and wave period, we are interested in knowing the solution structure of the weak oscillation state. It helps to understand the mechanism of amplitude death, and further improve dynamic stability of the floating airport by using the mechanism of amplitude death, having significant value for engineering safety design. With this motivation, we should derive the analytical solution of the weak oscillation state by using a simple harmonic averaging method (Xu et al., 2014b). Examining the governing Eq. (36) for the floating airport, there are two technical difficulties. The first is to deal with high-dimensional nonlinear differential equations, and the second is to deal with the complicated form of nonlinear coupling function.

For the nonlinear coupling function, we may expand it into a power series, given as

$$\Psi(\mathbf{X}_i,\mathbf{X}_j)\approx\sum_{n=0}^{N_T}\frac{1}{n!}\left[(\mathbf{X}_j-\mathbf{X}_{j0})\frac{\partial}{\partial\mathbf{X}_j}+(\mathbf{X}_i-\mathbf{X}_{i0})\frac{\partial}{\partial\mathbf{X}_i}\right]^n G(\mathbf{X}_{j0},\mathbf{X}_{i0}) \tag{37}$$

where $\Psi(\mathbf{X}_i,\mathbf{X}_j)$ denotes approximate coupling function and $\mathbf{X}_{j0},\mathbf{X}_{i0}$ indicate the coordinates of equilibrium position for the i,j-th modules respectively. N_T indicates the order of the Taylor's series. The detailed derivation of $\Psi(\mathbf{X}_i,\mathbf{X}_j)$ for the model explained in Eq. (36) in this paper can be found in Appendix. Then we obtain the approximate governing equation

$$(\mathbf{M}_i+\boldsymbol{\mu}_i)\ddot{\mathbf{X}}_i+\boldsymbol{\lambda}_i\dot{\mathbf{X}}_i+(\mathbf{K}_i+\mathbf{S}_i)\mathbf{X}_i=\mathbf{F}_{iW}\exp(-i\varphi_i)+\sum_{j=1}^{N}\Phi_{ij}\Psi(\mathbf{X}_i,\mathbf{X}_j),\quad i=1,\cdots,N \tag{38}$$

To deal with the high dimensional system, we rewrite Eq. (38) in a matrix form as

$$M\ddot{\mathbf{Y}}+C\dot{\mathbf{Y}}+\mathbf{K}\mathbf{Y}=\mathbf{f} \tag{39}$$

where

$$\mathbf{M}=\mathrm{dia}[\mathbf{M}_1+\boldsymbol{\mu}_1,\mathbf{M}_2+\boldsymbol{\mu}_2,\cdots,\mathbf{M}_N+\boldsymbol{\mu}_N],\mathbf{C}=\mathrm{dia}[\boldsymbol{\lambda}_1,\boldsymbol{\lambda}_2,\cdots,\boldsymbol{\lambda}_N],$$
$$\mathbf{K}=\mathrm{dia}[\mathbf{K}_1+\mathbf{S}_1,\mathbf{K}_2+\mathbf{K}_2,\cdots,\mathbf{K}_N+\mathbf{S}_N],\mathbf{Y}=[\mathbf{X}_1;\mathbf{X}_2;\cdots;\mathbf{X}_N],$$

$$\mathbf{f}=[\mathbf{F}_{1W}\exp(-i\varphi_1)+\sum_{j=1}^{N}\Phi_{1j}\Psi(\mathbf{X}_1,\mathbf{X}_j);\cdots;\mathbf{F}_{NW}\exp(-i\varphi_N)+\sum_{j=1}^{N}\Phi_{Nj}\Psi(\mathbf{X}_N,\mathbf{X}_j)].$$

Applying the averaging method, the solution of weak oscillation state which should be governed by the wave frequency ω is assumed as

$$\mathbf{Y}(t)=\mathbf{u}(t)\cos(\phi)+\mathbf{v}(t)\sin(\phi)$$
$$\dot{\mathbf{Y}}(t)=-\mathbf{u}(t)\omega\sin(\phi)+\mathbf{v}(t)\omega\cos(\phi) \tag{40}$$

where symbol $\phi=\omega t$ and $\mathbf{u},\mathbf{v}$ are the components of response amplitude, written as

$$\mathbf{u}(t)=[u_1,u_2,\cdots,u_N]^T,\qquad u_i=[u_{i1},u_{i2},u_{i3}]$$
$$\mathbf{v}(t)=[v_1,v_2,\cdots,v_N]^T,\qquad v_i=[v_{i1},v_{i2},v_{i3}] \tag{41}$$

assumed to be slow functions about time t. With the solution form in Eq. (40), we can deal with the high-dimensional system with the matrix form conveniently.

Differentiating the first equation of Eq. (40) with respect to the time t, we obtain

$$\dot{\mathbf{Y}}(t)=\dot{\mathbf{u}}(t)\cos(\phi)-\mathbf{u}(t)\omega\sin\phi+\dot{\mathbf{v}}(t)\sin\phi+\mathbf{v}(t)\omega\cos(\phi); \tag{42}$$

Substituting the second equation in Eq. (40) into Eq. (42), the resulting equation is

$$\dot{\mathbf{u}}(t)\cos\phi+\dot{\mathbf{v}}(t)\sin\phi=0 \tag{43}$$

Also differentiating the second equation of Eq. (40), we obtain

$$\ddot{\mathbf{Y}}(t)=-\dot{\mathbf{u}}(t)\omega\sin(\phi)-\mathbf{u}(t)\omega^2\cos\phi+\dot{\mathbf{v}}(t)\omega\cos(\phi)-\mathbf{v}(t)\omega^2\sin\phi; \tag{44}$$

Substituting the expressions about $\ddot{\mathbf{Y}}(t),\dot{\mathbf{Y}}(t)$ and $\mathbf{Y}(t)$ into Eq. (39), the following equation is found:

$$(M\dot{\mathbf{v}}\omega-\mathbf{M}\mathbf{u}\omega^2+\mathbf{C}\mathbf{v}\omega+\mathbf{K}\mathbf{u})\cos\phi-(M\dot{\mathbf{u}}\omega+\mathbf{M}\mathbf{v}\omega^2+\mathbf{C}\mathbf{u}\omega-\mathbf{K}\mathbf{v})\sin\phi$$
$$=\mathbf{F}(\mathbf{u},\mathbf{v},t) \tag{45}$$

Then, Eq. (43) is multiplied by $\mathbf{M}\omega\cos\phi$; Eq. (45) is multiplied by $-\sin\phi$. Adding the two equations, we obtained,

$$M\dot{\mathbf{u}}\omega=\left[(\mathbf{K}-\mathbf{M}\omega^2)\mathbf{v}-\mathbf{C}\mathbf{u}\omega\right]\sin^2\phi$$
$$+\left[(\mathbf{K}-\mathbf{M}\omega^2)\mathbf{u}+\mathbf{C}\mathbf{v}\omega\right]\cos\phi\sin\phi-\mathbf{F}\sin\phi \tag{46}$$

Assuming the variables u,v in Eq. (40) are slow functions about t, we take the average value along a period of variable ϕ as the true value by treating $\mathbf{u}$ and $\mathbf{v}$ as constants. The result turns out to be

$$\dot{\mathbf{u}} = \frac{\mathbf{M}^{-1}}{2\omega}\left[(\mathbf{K}-\mathbf{M}\omega^2)\mathbf{v}-\mathbf{C}\mathbf{u}\omega+\mathbf{q}^{(1)}\right] \tag{47}$$

Similarly, we obtain the average equation about $\mathbf{v}$, written as

$$\dot{\mathbf{v}} = -\frac{\mathbf{M}^{-1}}{2\omega}\left[(\mathbf{K}-\mathbf{M}\omega^2)\mathbf{u}+\mathbf{C}\mathbf{v}\omega+\mathbf{q}^{(2)}\right] \tag{48}$$

where

$$\mathbf{q}^{(k)} = [q_1^{(k)}, q_2^{(k)}, \cdots, q_N^{(k)}]^T, \qquad q_i^{(k)} = [q_{i1}^{(k)}, q_{i2}^{(k)}, q_{i3}^{(k)}], \qquad k=1,2$$

$$\mathbf{q}^{(1)} = -\frac{1}{\pi}\int_0^{2\pi} \mathbf{F}\,\sin\,\phi d\phi, \qquad \mathbf{q}^{(2)} = -\frac{1}{\pi}\int_0^{2\pi} \mathbf{F}\,\cos\,\phi d\phi.$$

In this way, the non-autonomous system Eq. (36) is converted into the autonomous system Eqs. (47) and (48) in the first-order ordinary differential equations. For a steady state of the autonomous system Eqs. (47) and (48) i.e. the amplitude death state, the necessary conditions are

$$\dot{\mathbf{u}} = \dot{\mathbf{v}} = 0 \tag{49}$$

Substituting Eq. (49) into Eqs. (47) and (48), a set of $4N$coupled nonlinear algebraic equations for $\mathbf{u}$ and $\mathbf{v}$ is obtained by

$$\Gamma(\mathbf{u},\mathbf{v},\varepsilon_1,\varepsilon_2) = \begin{bmatrix}(\mathbf{K}-\mathbf{M}\omega^2)\mathbf{v}-\mathbf{C}\mathbf{u}\omega+\mathbf{q}^{(1)} \\ (\mathbf{K}-\mathbf{M}\omega^2)\mathbf{u}+\mathbf{C}\mathbf{v}\omega+\mathbf{q}^{(2)}\end{bmatrix} = 0 \tag{50}$$

Right now, a generalized analytical solution for the network model of the floating airport has been formulated. The algebraic equations in Eq. (50) define a surface of oscillation amplitude in the parameter plane of the coupling strength. Referring to the solutions defined in Eq. (40), the response amplitudes of the i-th module, denoted by $A_{im}(m=1,2,3)$ respectively, can be expressed by

$$A_{im} = \sqrt{{u_{im}}^2+{v_{im}}^2}, \quad m=1,2,3 \tag{51}$$

Note that the solution of weak oscillation state defined by algebraic equations in Eq. (50) has to be solved through numerical approaches. The Newton-root-finding scheme can be employed for this task.

3.3. Mechanism and parameters domain of amplitude death

In this section, we use the analytical solution in Eq. (50) to view the response evolution of the floating airport when changing the coupling strength of rubber–cable connectors. This promises a direct illustration of the solution structure of Eq. (36) and then to analyze the mechanism of the occurrence of amplitude death.

Fig. 6 illustrates the surge amplitude of first two modules against the coupling strength k_c by using the analytical result in Eq. (50), where the parameter settings are the same as used for Fig. 4. We remark that the wave load is asymmetric because of the phase difference of the wave force imposed on each module and the fluid interaction between modules due to wave diffraction. The wave diffraction is ignored in the simple wave model, while the phase difference may result in a delay of motions among the modules but does not affect the response amplitudes of the modules. This feature is also observed in our numerical simulations (but not illustrated in this paper). Thus the response amplitudes of the module 1 and module 2 in Fig. 6 are identical to that of the module 5 and module 4 respectively due to the symmetry of the structure. In Fig. 6(a), the solution structure for the system contains two inclined resonance peaks and indicates multiple solution branches. When the coupling strength k_c increases forward, the system first stays at the lower branch (dark solid line) where the response curve corresponds to relatively small amplitude that is regarded as weak oscillation state. When the coupling strength k_c reaches to a critical value

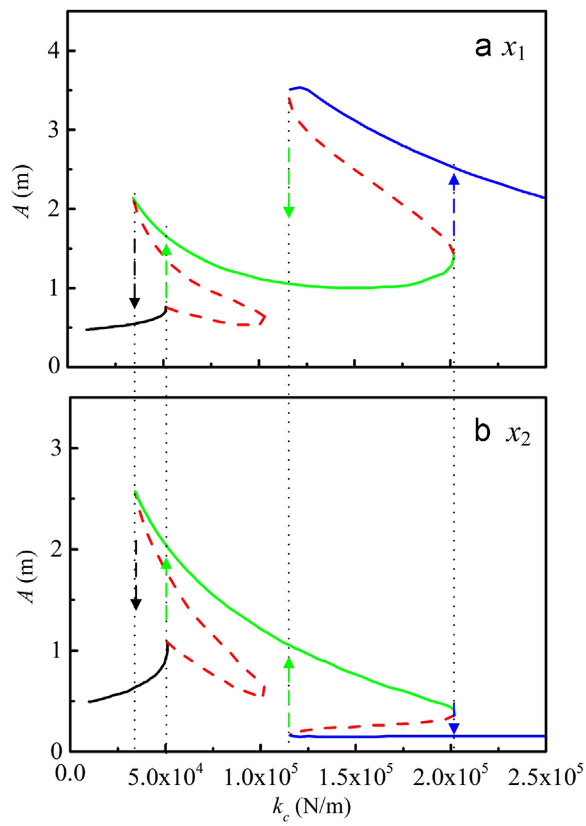

Fig. 6. Resonance curves versus the coupling strength of surge motion for (a) first module and (b) second module with wave period $T=10\ s$ (Solid line denotes stable solution, dash line illustrates unstable solution, and arrow line indicates jumping direction). (For interpretation of the references to color in this figure, the reader is referred to the web version of this article.)

$k_c = 5.001 \times 10^4$, the system state leaps up to the upper branch (green solid line) where the response curve appears to be a large amplitude. We refer this critical value as jump up (arrow up). On the contrary, when the coupling strength k_c is decreased backwards, the system initially remains on the upper branch curve until a drop down transition (arrow down) occurs. It is worth to note that the jump up and drop down phenomena can induce a rapid change of the response amplitude. Between the different solution branches, the dash-line curve indicates the unstable solution which cannot be observed by numerical simulations.

Comparing Fig. 6(a) and (b), the solution structures also indicate that the jumping phenomena always happen among all motions simultaneously at the same critical value. Fig. 6 reveals such a fact that the amplitude death is terminated suddenly because the weak oscillation solution branch ends up at jump up point leaping to the upper solution branch with large oscillations. This mechanism is very different from that of Hopf bifurcation (Zhai et al., 2004) or Saddle-node bifurcation (Karnatak et al., 2010) in autonomous systems. Thus jump up event plays a key role on the cease of the amplitude death, and the critical condition for this event is the boundary condition of amplitude death state.

Fig. 6 shows the whole picture of the all solution branches in the stiffness range of $10^3 < k_c < 2.5 \times 10^5\ N/m$ (stable and unstable solutions) using an analytical method, which can match up with the numerical solution of Fig. 4 in the stiffness range of $10^3 < k_c < 1 \times 10^5\ N/m$. The weak oscillation state in the region $k_c < 4.71 \times 10^4\ N/m$ in Fig. 4 corresponds to the solution branch marked by black solid line in Fig. 6. The jump up point $k_c = 4.71 \times 10^4\ N/m$ in Fig. 4 corresponds to the first upward green arrow line in Fig. 6. The high-rise responses after the first jump in Fig. 4 is associated

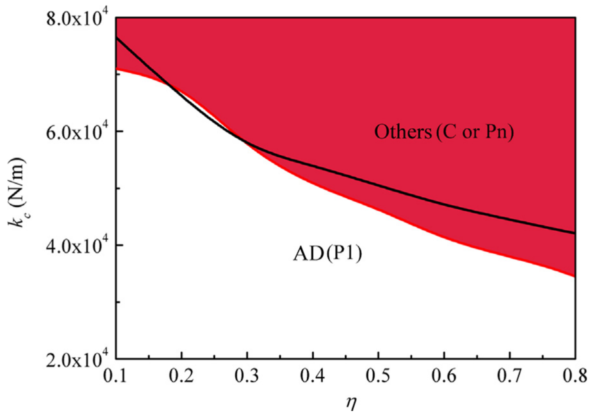

Fig. 7. Region for amplitude death in parameter space $(k_c, \eta)$for $N=5$with wave period $T=10\ s$ (AD: amplitude death; Others: large oscillation state; P1: period-1 motion; C or Pn: chaotic or high-order period motion; Black solid line: the boundary for AD by the analytical criterion). (For interpretation of the references to color in this figure, the reader is referred to the web version of this article.)

with the high-rise solution branch in Fig. 6, marked in green solid line. Note that the amplitudes in large oscillation region after jumping have some discrepancy for the two methods. The reason is that the analytical method assumes only one harmonic component for the response solution but the actual response may involve a combination of multiple harmonic components. Nevertheless, our main purpose is to predict the jump point for determining the AD boundary and the results from the analytical solution are sufficient for us to carry out the task.

Concerning the global stability of a large scale floating airport, the determination for the boundary condition of amplitude death is of the most interest. The mathematic condition for the jumping point in Eq. (50) can be determined by using the implicit-function theorem (Kubíček and Klíč, 1983), namely

$$\overline{\Gamma}(\mathbf{u}, \mathbf{v}, \varepsilon_1, \varepsilon_2) = \det\mathbf{J}\,(\mathbf{u}, \mathbf{v}, \varepsilon_1, \varepsilon_2) = 0 \tag{52}$$

where $\mathbf{J}$ indicates the Jacobian matrix of function Γ. Eq. (52) is the critical condition for the boundary of amplitude death. From Eq. (50), the Jacobian matrix can be expressed as

$$\mathbf{J} = \mathbf{J_A} + \mathbf{J_D} \tag{53}$$

where $\mathbf{J_A}, \mathbf{J_D}$ is the Jacobian matrix for the linear and nonlinear part of function Γ, written as

$$\mathbf{J_A} = \begin{bmatrix} -\mathbf{C}\omega & \mathbf{K}-\mathbf{M}\omega^2 \\ \mathbf{K}-\mathbf{M}\omega^2 & \mathbf{C}\omega \end{bmatrix}, \quad \mathbf{J_D} = \begin{bmatrix} \frac{\partial \mathbf{q}^{(1)}}{\partial \mathbf{u}} & \frac{\partial \mathbf{q}^{(1)}}{\partial \mathbf{v}} \\ \frac{\partial \mathbf{q}^{(2)}}{\partial \mathbf{u}} & \frac{\partial \mathbf{q}^{(2)}}{\partial \mathbf{v}} \end{bmatrix} \tag{54}$$

Fig. 7 shows the region of the amplitude death, the white area marked with ‘AD(P1)’, from the numerical scanning in the space of coupling strength ratio η and coupling strength k_c for wave period $T=10\ s$. The red region marked with ‘Others(C or Pn)’ relates to large oscillation state. The analytical critical condition explained in Eq. (52) plotted with black solid curve lies closely between the white and red regions. For this example, the amplitude death domain occupies the downside region. In comparison, there is insignificant discrepancy between the analytical and numerical results. Fig. 7 is only a glance of the special dynamic behavior of the suppressed weak oscillatory state in terms of coupling strengths. Surely, the existence of the amplitude death phenomenon may be affected by other parameters, such as wave period, wave height and the number of floating modules coupled in the system, etc. For a stationarity design of the floating airport, it needs a tremendous effort to produce a series of AD diagrams with covering all the key parameters. In general, the proposed analytical criterion can reasonably predict the region boundary of amplitude death. The significance of deriving the critical condition for amplitude death is that it can greatly reduce the effort to determine the design region of amplitude death, while numerical approach is very time consuming.

We remark that the state of amplitude death corresponds to the weak oscillation state of non-autonomous systems. This typical dynamic phenomenon of amplitude death only exists in nonlinear network-like dynamic systems. We introduce the concept of the amplitude death aiming to determine the parametric region for the global dynamic stability of the floating airport. This work is important for retaining the large scale marine system in a stationary state and keeping the connector load at low levels.

4. Summary and conclusions

In this paper, a novel methodology is proposed to investigate the dynamic characteristic and global stability of the floating airport. A multi-module network model of large scale floating airport is developed based on linear wave theory, a dynamic model of single floating module, a coupling model of a new connector and constraint model of a mooring system. We revealed a typical phenomenon of amplitude death of the airport model, a weak oscillation state, and stated its significant role in the safety design of the floating airport. A semi-analytical method is presented to analyze the mechanism of amplitude death which is a new feature compared with our recent work (Zhang et al., 2015). The results show that the transition of amplitude death is due to jumping events among different solution branches and a criterion was derived for determining the boundary of amplitude death region. We illustrate a numerical example to explore the amplitude death region for the floating airport in a parameter domain spanned by stiffness ratio and cable stiffness. Meanwhile we verified the correctness of analytic criterion of amplitude death. The results coincide well. The analytical condition allows to quickly find the parametric region for the global dynamic stability of the floating airport and avoids tedious numerical search. This work is an application of the network theory in marine engineering. The methodology can be widely used for other engineering problems with network structures.

Acknowledgments

This research work was supported by the 973 research Grant (2013CB036104) and the National Natural Science Foundation of China, PR China (11472100).

Appendix

To deal with the complex form of the coupling function in Eq. (36), we expand the nonlinear function by a power series until third order, given as

$$\overline{G}_2(\mathbf{X}_i, \mathbf{X}_j) = \begin{cases} \begin{bmatrix} \Delta\bar{l}_{ijx} & \Delta\bar{l}_{ijz} & \Delta\bar{l}_{ij\beta} \end{bmatrix}^T & \mathrm{sgn}(j-i)(x_j-x_i) \geq 0 \\ \begin{bmatrix} 0 & 0 & 0 \end{bmatrix}^T & \mathrm{sgn}(j-i)(x_j-x_i) < 0 \end{cases} \tag{A.1}$$

where

$$\Delta\bar{l}_{ijx} = \left[L^2\mathrm{sgn}(j-i)/(2\delta)\beta_j\beta_i + L/\delta\left(\beta_j+\beta_i\right)(z_j-z_i)\right] + \left[2-\left(L/\delta\right)^2\beta_j\beta_i - 2L\mathrm{sgn}(j-i)/\delta^2\left(\beta_j+\beta_i\right)(z_j-z_i)\right](x_j-x_i),$$

$$\Delta\bar{l}_{ijz} = \left[\left(3L^2/(2\delta^2)+\left(\delta_2/\delta\right)^2\right)\beta_j\beta_i\right](z_j-z_i) + \left[L/\delta\left(\beta_j+\beta_i\right) + \left(2\mathrm{sgn}(j-i)/\delta - 3(3L^2+2{\delta_2}^2)/\delta^2\beta_j\beta_i\right)(z_j-z_i)\right](x_j-x_i),$$

$$\Delta \bar{l}_{ij\beta} = \frac{{\delta_2}^2}{2}(\beta_j - \beta_i) - \left[\frac{\mathrm{sgn}(j-i)(3L^3 + 2L^2\delta + 2L{\delta_2}^2 + 2\delta{\delta_2}^2)}{4\delta^2}\beta_j\beta_i\right](z_j - z_i)$$
$$+ \left[-L^2 \mathrm{sgn}(j-i)/(2\delta)\beta_j - \left(L\mathrm{sgn}(j-i) + L^2\mathrm{sgn}(j-i)/(2\delta)\right)\beta_i\right.$$
$$\left. + \left(-L/\delta + (9L^3 + 4L^2\delta + 6L{\delta_2}^2 + 4\delta{\delta_2}^2)/(4\delta^3)\beta_j\beta_i\right)(z_j - z_i)\right](x_j - x_i).$$

The power series expressions are still complex and so we continue to simply the expressions. The pith angle β is a little quantity compared with other freedoms, so we ignore the $\beta_i\beta_j$. Considering the scale of the floating, there have $L\mathrm{sgn}(j-i) \ll L^2\mathrm{sgn}(j-i)/(2\delta)$, so we ignore the term $L\mathrm{sgn}(j-i)\beta_i$ in expression of $\Delta \bar{l}_{ij\beta}$. Thus, the coupling form can be formulated as

$$G_2^s(\mathbf{X}_i, \mathbf{X}_j) = \begin{cases} \begin{bmatrix} \Delta l_{ijx}^s & \Delta l_{ijz}^s & \Delta l_{ij\beta}^s \end{bmatrix}^T & \mathrm{sgn}(j-i)(x_j - x_i) \ge 0 \\ \begin{bmatrix} 0 & 0 & 0 \end{bmatrix}^T & \mathrm{sgn}(j-i)(x_j - x_i) < 0 \end{cases} \tag{A.2}$$

where

$$\Delta l_{ijx}^s = L(\beta_j + \beta_i)(z_j - z_i)/\delta + \left[2 - 2L\mathrm{sgn}(j-i)/\delta^2(\beta_j + \beta_i)(z_j - z_i)\right](x_j - x_i),$$
$$\Delta l_{ijz}^s = \left[L/\delta(\beta_j + \beta_i) + 2\mathrm{sgn}(j-i)/\delta(z_j - z_i)\right](x_j - x_i),$$
$$\Delta l_{ij\beta}^s = {\delta_2}^2/2(\beta_j - \beta_i) - \left[L^2\mathrm{sgn}(j-i)/(2\delta)(\beta_j + \beta_i) + L/\delta(z_j - z_i)\right](x_j - x_i).$$

Thus the approximate coupling function for the rubber-cable connector can be written as

$$\Psi(\mathbf{X}_i, \mathbf{X}_j) = \begin{cases} \varepsilon_1 \begin{bmatrix} (x_j - x_i)^3 & 0 & 0 \end{bmatrix}^T & \mathrm{sgn}(j-i)(x_j - x_i) < 0 \\ \varepsilon_2 \begin{bmatrix} \Delta l_{ijx}^s & \Delta l_{ijz}^s & \Delta l_{ij\beta}^s \end{bmatrix}^T & \mathrm{sgn}(j-i)(x_j - x_i) \ge 0 \end{cases} \tag{A.3}$$

References

Aoki, S., 1997. Shallow water effect on hydrodynamic coefficients of very large floating structures. In: Proceedings of 7th International Offshore Polar Engineering Conference. pp. 253–260.

Armstrong, E.R., 1924. Sea station. Patent no. 1511153. ⟨http://www.google.com/patents/US1511153⟩.

Armstrong, E.R., 1943. The Seadrome Project for Transatlantic Airways. Seadrome Patents Co., Wilmington.

Bar-Eli, K., 1984. Coupling of chemical oscillators. J. Phys. Chem. 88, 3616–3622. http://dx.doi.org/10.1021/j150660a048.

Bhattacharya, B., Fujikubo, M., Hudson, D.A., Riggs, H.R., Seto, H., Shin, H., Shugar, T. A., Yasuzawa, Y., Zong, Z., 2006. Very large floating structures. In: Proceedings of the16th International Ship and Offshore Structures Congress. Southampton, pp. 391–442.

Chen, X.J., Cui, W.C., Shen, Q., 2001. New method for predicting the motion responses of a flexible joint multi-body floating system to irregular waves. China Ocean Eng. 15, 491–498. http://dx.doi.org/10.3321/j.issn:0890-5487.2001.04.004.

Cui, W.C., Yang, J.M., Wu, Y.S., Liu, Y.Z., 2007. Theory of Hydroelasticity and Its Application to Very Large Floating Structure. Jiao Tong University Press, Shanghai.

Du, S.X., Ertekin, C.R., 1991. Dynamic response analysis of a flexibly joined, multi-module very large floating structure. IEEE Proc. OCEANS 91, 1286–1293. http://dx.doi.org/10.1109/OCEANS.1991.606474.

Faltinsen, O.M., 1996. Bottom slamming on a floating airport. In: Proceedings of the International Workshop on Very Large Floating Structures (VLFS'96), Ship Research Institute, Tokyo, Japan. pp. 97–106.

Fu, S.X., Moan, T., Chen, X.J., Cui, W.C., 2007. Hydroelastic analysis of flexible floating interconnected structures. Ocean Eng. 34, 1516–1531. http://dx.doi.org/10.1016/j.oceaneng.2007.01.003.

Gao, R.P., Tay, Z.Y., Wang, C.M., Koh, C.G., 2011. Hydroelastic response of very large floating structure with a flexible line connection. Ocean Eng. 38, 1957–1966. http://dx.doi.org/10.1016/j.oceaneng.2011.09.021.

Hamamoto, T., 1994. Dynamic response of flexible circular floating islands subjected to stochastic waves. In: Proceedings of International Conference Hydro-Elasticity Marine Technology. pp. 433–445.

Hong, S.Y., Choi, Y.R., Kim, D.J., Kim, M.H., 1999. Responses of a barge-mounted platform in waves and currents. Int. J. Offshore Polar Eng. 9, 283–292.

Jain, R.K., 1980. A simple method of calculating the equivalent stiffnesses in mooring cables. Appl. Ocean Res. 2, 139–142. http://dx.doi.org/10.1016/0141-1187(80)90006-1.

Kaneko, K., 1993. Theory and Applications of Coupled Map Lattices. Wiley, New Youk.

Karnatak, R., Punetha, N., Prasad, A., Ramaswamy, R., 2010. Nature of the phase-flip transition in the synchronized approach to amplitude death. Phys. Rev. E 82, 46219. http://dx.doi.org/10.1103/PhysRevE.82.046219.

Kashiwagi, M., 1998. A B-spline Galerkin scheme for calculating the hydroelastic response of a very large floating structure in waves. J. Mar. Sci. Technol. 3, 37–49. http://dx.doi.org/10.1007/BF01239805.

Kerman, B.R., 1988. Sea Surface Sound: Natural Mechanisms of Surface Generated Noise in the Ocean. Springer Science & Business Media.

Khabakhpasheva, T.I., Korobkin, A.A., 2001. Reduction of hydroelastic response of floating platform in waves. In: Proceedings of 16th Internationall WkspWater Waves Floating Bodies. Hiroshima, Japan, pp. 73–76.

Kim, J.W., Ertekin, R.C., 1998. An eigenfunction-expansion method for predicting hydroelastic behaviour of a shallow-drift VLFS. In: Kashiwagi, M., Koterayama, W., Ohkusu, M. (Eds.), Proceedings of 2nd Hydro-Elasticity Marine Technology. Kyushu University, Fukuoka, Japan, Fukuoka, Japan, pp. 47–59.

Koh, H.S., Lim, Y.B., 2009. The floating platform at the Marina Bay, Singapore. Struct. Eng. Int. 19, 33–37. http://dx.doi.org/10.2749/101686609787398263.

Konishi, K., 2003. Amplitude death induced by dynamic coupling. Phys. Rev. E 68, 67202. http://dx.doi.org/10.1103/PhysRevE.68.067202.

Kubíček, M., Klíč, A., 1983. Direction of branches bifurcating at a bifurcation point. Determination of starting points for a continuation algorithm. Appl. Math. Comput. 13, 125–142. http://dx.doi.org/10.1016/0096-3003(83)90034-6.

Lee, C.H., Newman, J.N., 2000. An assessment of hydroelasticity for very large hinged vessels. J. Fluids Struct. 14, 957–970. http://dx.doi.org/10.1006/jfls.2000.0305.

Maeda, H., Maruyama, S., Inoue, R., Watanabe, K., Togawa, S., Suzuki, F., 1979. On the motions of a floating structure which consists of two or three blocks with rigid or pin joints. J. Soc. Nav. Archit. Jpn. 1979, 71–78. http://dx.doi.org/10.2534/jjasnaoe1968.1979.71.

Ogawa, Y., 1984. Fundamental analysis of deep sea mooring line in static equilibrium. Appl. Ocean Res. 6, 140–147. http://dx.doi.org/10.1016/0141-1187(84)90003-8.

Ott, E., 2002. Chaos in Dynamical Systems. Cambridge University Press, Cambridge.

Pecora, L.M., Carroll, T.L., 1990. Synchronization in chaotic systems. Phys. Rev. Lett. 64, 821–824. http://dx.doi.org/10.1002/3527607455.ch11.

Pinkster, J.A., Fauzi, A., 1997. The effect of air cushions under floating offshore structures. In: Proceedings of the Eighth International Conference on the Behavior of Offshore Structure. pp. 143–158.

Resmi, V., Ambika, G., Amritkar, R.E., 2011. General mechanism for amplitude death in coupled systems. Phys. Rev. E 84, 46212. http://dx.doi.org/10.1103/PhysRevE.84.046212.

Riggs, H.R., Ertekin, R.C., 1993. Approximate methods for dynamic response of multi-module floating structures. Mar. Struct. 6, 117–141. http://dx.doi.org/10.1016/0951-8339(93)90016-V.

Riggs, H.R., Ertekin, R.C., Mills, T.R.J., 1999. Impact of connector stiffness on the response of a multi-module mobile offshore base. Int. J. Offshore Polar Eng. 9, 126–133.

Rognaas, G., Xu, J., Lindseth, S., Rosendahl, F., 2001. Mobile offshore base concepts. Concrete hull and steel topsides. Mar. Struct. 14, 5–23. http://dx.doi.org/10.1016/S0951-8339(00)00019-8.

Sannasiraj, S.A., Sundar, V., Sundaravadivelu, R., 1998. Mooring forces and motion responses of pontoon-type floating breakwaters. Ocean Eng. 25, 27–48. http://dx.doi.org/10.1016/S0029-8018(96)00044-3.

Sannasiraj, S.A., Sundaravadivelu, R., Sundar, V., 2001. Diffraction–radiation of multiple floating structures in directional waves. Ocean Eng. 28, 201–234. http://dx.doi.org/10.1016/S0029-8018(99)00066-9.

Saxena, G., Prasad, A., Ramaswamy, R., 2012. Amplitude death: the emergence of stationarity in coupled nonlinear systems. Phys. Rep. 521, 205–228. http://dx.doi.org/10.1016/j.physrep.2012.09.003.

Stoker, J.J., 2011. Water Waves: The Mathematical Theory with Applications. Wiley-Interscience.

Strogatz, S.H., 1998. Nonlinear dynamics: death by delay. Nature 394, 316–317. http://dx.doi.org/10.1038/28488.

Taghipour, R., Perez, T., Moan, T., 2008. Hybrid frequency–time domain models for dynamic response analysis of marine structures. Ocean Eng. 35, 685–705. http://dx.doi.org/10.1016/j.oceaneng.2007.11.002.

Taylor, R.E., Waite, J.B., 1978. The dynamics of offshore structures evaluated by boundary integral techniques. Int. J. Numer. Methods Eng. 13, 73–92. http://dx.doi.org/10.1002/nme.1620130106.

Wang, C.M., Tay, Z.Y., 2011. Very large floating structures: applications, research and development. Procedia Eng. 14, 62–72. http://dx.doi.org/10.1016/j.proeng.2011.07.007.

Watanabe, E., Utsunomiya, T., Wang, C.M., 2004. Hydroelastic analysis of pontoon-type VLFS: a literature survey. Eng. Struct. 26, 245–256. http://dx.doi.org/10.1016/j.engstruct.2003.10.001.

Winkler, R.S., Seidl, L.H., Riggs, H.R., 1990. The Design and Analysis of Very Large Floating Structures. Department of Ocean Engineering, University of Hawaii, Hawaii.

Xu, D.L., Zhang, H.C., Lu, C., Qi, E.R., Hu, J.J., Wu, Y.S., 2014a. On study of nonlinear network dynamics of flexibly connected multi-module very large floating structures, Vulnerability, Uncertainty, and Risk. American Society of Civil Engineers, Reston, VA, pp. 1805–1814. http://dx.doi.org/10.1061/9780784413609.181, In:

Xu, D.L., Zhang, H.C., Lu, C., Qi, E.R., Tian, C., Wu, Y.S., 2014b. Analytical criterion for amplitude death in nonautonomous systems with piecewise nonlinear coupling. Phys. Rev. E 89, 42906. http://dx.doi.org/10.1103/PhysRevE.89.042906.

Xu, D.L., Lu, C., Zhang, H.C., 2014c. Dynamic modeling and nonlinear characteristics of floating airport. Chin. J. Theor. Appl. Mech. 47, 289–330. http://dx.doi.org/10.6052/0459-1879-14-138.

Zhai, Y., Kiss, I., Hudson, J., 2004. Amplitude death through a Hopf bifurcation in coupled electrochemical oscillators: experiments and simulations. Phys. Rev. E 69, 26208. http://dx.doi.org/10.1103/PhysRevE.69.026208.

Zhang, H.C., Xu, D.L., Lu, C., Qi, E.R., Hu, J.J., Wu, Y.S., 2015. Amplitude death of a multi-module floating airport. Nonlinear Dyn. 79, 2385–2394. http://dx.doi.org/10.1007/s11071-014-1819-x.

Zheng, Y.H., You, Y.G., Shen, Y.M., 2004. On the radiation and diffraction of water waves by a rectangular buoy. Ocean Eng. 31, 1063–1082. http://dx.doi.org/10.1016/j.oceaneng.2003.10.012.